NeuroImage 285 (2024) 120481

Contents lists available at ScienceDirect

NeuroImage

journal homepage: www.elsevier.com/locate/ynimg

Connectome-wide structure-function coupling models implicate polysynaptic alterations in autism

Bo-yong Park [a,b,c,d,*], Oualid Benkarim [a], Clara F. Weber [a], Valeria Kebets [a], Serena Fett [a], Seulki Yoo [e], Adriana Di Martino [f], Michael P. Milham [f], Bratislav Misic [a], Sofie L. Valk [g], Seok-Jun Hong [a,d,f,h], Boris C. Bernhardt [a,**]

[a] McConnell Brain Imaging Centre, Montreal Neurological Institute and Hospital, McGill University, Montreal, QC, Canada
[b] Department of Data Science, Inha University, Incheon, South Korea
[c] Department of Statistics and Data Science, Inha University, Incheon, South Korea
[d] Center for Neuroscience Imaging Research, Institute for Basic Science, Suwon, South Korea
[e] Convergence Research Institute, Sungkyunkwan University, Suwon, South Korea
[f] Center for the Developing Brain, Child Mind Institute, New York, United States
[g] Max Planck Institute for Human Cognitive and Brain Sciences, Leipzig, Germany
[h] Department of Biomedical Engineering, Sungkyunkwan University, Suwon, South Korea

ARTICLE INFO

Keywords:
Autism
Structure-function coupling
Diffusion time
Synaptic communication

ABSTRACT

Autism spectrum disorder (ASD) is one of the most common neurodevelopmental diagnoses. Although incompletely understood, structural and functional network alterations are increasingly recognized to be at the core of the condition. We utilized multimodal imaging and connectivity modeling to study structure-function coupling in ASD and probed mono- and polysynaptic mechanisms on structurally-governed network function. We examined multimodal magnetic resonance imaging data in 80 ASD and 61 neurotypical controls from the Autism Brain Imaging Data Exchange (ABIDE) II initiative. We predicted intrinsic functional connectivity from structural connectivity data in each participant using a Riemannian optimization procedure that varies the times that simulated signals can unfold along tractography-derived personalized connectomes. In both ASD and neurotypical controls, we observed improved structure-function prediction at longer diffusion time scales, indicating better modeling of brain function when polysynaptic mechanisms are accounted for. Prediction accuracy differences (Δprediction accuracy) were marked in transmodal association systems, such as the default mode network, in both neurotypical controls and ASD. Differences were, however, lower in ASD in a polysynaptic regime at higher simulated diffusion times. We compared regional differences in Δprediction accuracy between both groups to assess the impact of polysynaptic communication on structure-function coupling. This analysis revealed that between-group differences in Δprediction accuracy followed a sensory-to-transmodal cortical hierarchy, with an increased gap between controls and ASD in transmodal compared to sensory/motor systems. Multivariate associative techniques revealed that structure-function differences reflected inter-individual differences in autistic symptoms and verbal as well as non-verbal intelligence. Our network modeling approach sheds light on atypical structure-function coupling in autism, and suggests that polysynaptic network mechanisms are implicated in the condition and that these can help explain its wide range of associated symptoms.

1. Introduction

Autism spectrum disorder (ASD) is a common neurodevelopmental diagnosis encompassing atypical social and communication abilities, repetitive behaviors and interests, and sometimes altered sensory and perceptual processing as well as imbalances in verbal and non-verbal abilities (Christensen et al., 2018; Hong et al., 2022, 2020; Mottron et al., 2006). While biological underpinnings remain incompletely

* Corresponding author at: Department of Data Science, Inha University, Incheon, South Korea.
** Corresponding author at: Multimodal Imaging and Connectome Analysis Lab, McConnell Brain Imaging Centre, Montreal Neurological Institute, McGill University, Montreal, Quebec, Canada.
E-mail addresses: boyong.park@inha.ac.kr (B.-y. Park), boris.bernhardt@mcgill.ca (B.C. Bernhardt).

https://doi.org/10.1016/j.neuroimage.2023.120481
Received 20 May 2023; Received in revised form 29 November 2023; Accepted 1 December 2023
Available online 2 December 2023

understood, convergent evidence supports a key role of atypical brain networks. Indeed, there is now an increasing catalog of ASD-related genes and pathways involved in synaptic and circuit organization (Geschwind, 2011; Quesnel-Vallières et al., 2019; Rylaarsdam and Guemez-Gamboa, 2019). Moreover, several histopathological studies suggest dendritic reorganization (Hutsler and Zhang, 2010; Martínez-Cerdeño, 2017), alterations in cortical lamination (Hutsler et al., 2007; Simms et al., 2009), and atypical columnar layout in individuals with ASD (Amaral et al., 2008; McKavanagh et al., 2015). Molecular and circuit findings are complemented by *in vivo* magnetic resonance imaging (MRI) studies, suggesting atypical structural and functional network organization, often pointing to a mosaic pattern of increased and decreased connectivity in ASD (Di Martino et al., 2014; Hong et al., 2019b; Kana et al., 2014; Müller et al., 2011; Uddin et al., 2013). Recent studies have represented structural and functional network organization in compact connectivity spaces, identified via unsupervised dimensionality reduction techniques, and tracked typical and atypical development (Hong et al., 2019a; Huntenburg et al., 2018; Margulies et al., 2016; Park et al., 2021b, 2022; Tian et al., 2020). In neurotypical adults, these techniques have robustly identified main spatial axes corresponding to the functional cortical hierarchy, differentiating sensory and motor systems interacting with the outside world from transmodal networks, such as default-mode and limbic networks, implicated in higher-order and social cognition (Bernhardt et al., 2022; Margulies et al., 2016; Paquola et al., 2022; Smallwood et al., 2021; Sydnor et al., 2021). Translating this framework to ASD, increasing evidence suggests a reduced hierarchical differentiation between sensory/motor and transmodal systems both at the level of structural and functional connectivity, which have been shown to relate to autism risk gene expression patterns (Park et al., 2021b). Overall, findings suggest that ASD perturbs neural circuit organization across multiple, likely interacting spatial scales.

A key assumption of neuroscience is that brain structure and function are intertwined. Expanding from experimental explorations in non-human animals, imaging studies in neurotypical populations have addressed structure-function coupling in the living human brain (Baum et al., 2020; Honey et al., 2009; Mišic et al., 2016; Park et al., 2021d; Snyder and Bauer, 2019; Suárez et al., 2020; Vázquez-Rodríguez et al., 2019). Generally, such work seeks to identify a mapping from structural connectivity (approximated via diffusion MRI tractography) to functional connectivity (estimated via functional MRI signal correlations). Approaches include statistical associative techniques, biophysical modeling, and graph communication models (Avena-Koenigsberger et al., 2019, 2018; Bazinet et al., 2021; Becker et al., 2018; Breakspear, 2017; Deco et al., 2013; Goñi et al., 2014; Honey et al., 2009; Mišic et al., 2016; Rosenthal et al., 2018; Seguin et al., 2018; Wang et al., 2019). This body of work emphasizes that functional interactions unfold both along direct monosynaptic connections as well as indirect polysynaptic pathways (Damoiseaux and Greicius, 2009; Goñi et al., 2014; Honey et al., 2009; Seguin et al., 2019; Suárez et al., 2020). In neurotypical adults, our team recently proposed a novel approach to simulate functional interactions from structural connectivity with high fidelity and at an individual-participant level (Benkarim et al., 2022). This work derived low-dimensional eigenspaces from a structural connectome, on which virtual signal diffusion models were then used to predict inter-regional functional interactions. These diffusion processes unfold along existing connections and are governed by a free diffusion time parameter, with higher diffusion times implicating an increasing contribution of indirect pathways to functional interactions. In other words, this Riemannian manifold optimization framework can parameterize the impact of polysynaptic communication on global structure-function coupling. At a regional scale, comparing simulations with empirically measured data showed that while functional interactions of sensory and motor systems can be adequately modeled with only a limited number of synaptic steps, accurate simulations of interactions of transmodal systems require longer time scales, and thus a more polysynaptic regime. As such, mono- and polysynaptic communication mechanisms underpinning structure-function coupling in healthy individuals can be compactly described along an unimodal to transmodal brain hierarchy.

Our study examined structure-function relations in autism and explored the differential impact of mono- *vs* polysynaptic communication. Core to our approach was a Riemannian optimization and modeling framework (Benkarim et al., 2022), which has shown state-of-the-art performance in predicting functional interactions from structural connectivity data in single neurotypical individuals. We studied global and region-specific differences in prediction accuracy across diffusion times in individuals with ASD and neurotypicals to evaluate the impact of mono- and polysynaptic network communication. The topography of ASD-related alterations was spatially associated with canonical features of macroscale functional organization, namely intrinsic functional systems and sensory-transmodal cortical hierarchical gradients. Using partial least squares regression, we finally associated ASD-related alterations with autistic symptoms and measures of verbal/non-verbal intelligence to explore how atypical structure-function coupling reflects behavioral phenotypes.

2. Methods

2.1. Study participants

We studied 141 participants (80 ASD, 61 neurotypicals) obtained from three independent sites of (1) New York University Langone Medical Center (NYU), (2) Trinity College Dublin (TCD), and (3) San Diego State University (SDSU) from the Autism Brain Imaging Data Exchange initiative (ABIDE-II; https://fcon_1000.projects.nitrc.org/indi/abide) (Di Martino et al., 2017). Inclusion criteria were: (i) sites included children and adults with autism and controls with $\geq$10 individuals per group, (ii) multimodal MRI data (*i.e.,* T1-weighted, resting-state functional MRI (rs-fMRI), and diffusion MRI) available, (iii) acceptable cortical surface extraction on T1-weighted MRI, (iv) low head motion in the rs-fMRI time series (*i.e.,* >0.3 mm framewise displacement). Individuals with ASD were diagnosed by an in-person interview with clinical experts and gold standard instruments from the Autism Diagnostic Observation Schedule (ADOS) (Lord et al., 2000) and/or Autism Diagnostic Interview-Revised (ADI-R) (Lord et al., 1994). Neurotypical controls did not have any history of mental disorders. For all groups, participants who had genetic disorders associated with autism (*i.e.,* Fragile X), contraindications to MRI scanning, and who were pregnant were excluded. Detailed demographic information of the participants is reported in **Supplementary Table 1**. ABIDE data collections were performed in accordance with local Institutional Review Board guidelines. In accordance with HIPAA guidelines and 1000 Functional Connectomes Project/INDI protocols, all ABIDE datasets have been fully anonymized, with no protected health information included.

2.2. MRI acquisition

The data from the three included sites were as follows:

(i) NYU: Imaging data were acquired using a 3T Siemens Allegra scanner. The T1-weighted data were obtained using a 3D magnetization prepared rapid acquisition gradient echo (MPRAGE) sequence (repetition time (TR) = 2530 ms; echo time (TE) = 3.25 ms; inversion time (TI) = 1100 ms; flip angle = 7°; matrix = 256 × 192; and voxel size = 1.3 × 1.0 × 1.3 mm^3). The rs-fMRI data were acquired using a 2D echo planar imaging (EPI) sequence (TR = 2000 ms; TE = 15 ms; flip angle = 90°; matrix = 80 × 80; number of volumes = 180; and voxel size = 3.0 × 3.0 × 4.0 mm^3). The diffusion MRI data were obtained using a 2D spin-echo EPI (SE-EPI) sequence (TR = 5200 ms; TE = 78 ms; matrix =

64 × 64; voxel size = 3 mm^3 isotropic; 64 directions; b-value = 1000 s/mm^2; and 1 b0 image).

(ii) TCD: Imaging data were acquired using a 3T Philips Achieva scanner. The T1-weighted MRI were acquired using a 3D MPRAGE (TR = 8400 ms; TE = 3.90 ms; TI = 1150 ms; flip angle = 8°; matrix = 256 × 256; voxel size = 0.9 mm^3 isotropic). The rs-fMRI data were acquired using a 2D EPI (TR = 2000 ms; TE = 27 ms; flip angle = 90°; matrix = 80 × 80; number of volumes = 210; and voxel size = 3.0 × 3.0 × 3.2 mm^3). The diffusion MRI data were acquired using a 2D SE-EPI (TR = 20,244 ms; TE = 79 ms; matrix = 124 × 124; voxel size = 1.94 × 1.94 × 2 mm^3; 61 directions; b-value = 1500 s/mm^2; and 1 number b0 image).

(iii) SDSU: Imaging data were acquired using a GE 3T MR750 scanner. The T1-weighted MRI were acquired using a 3D fast spoiled gradient echo (FSPGR) (TR = 8136 ms; TE = 3.172 ms; TI = 600 ms; flip angle = 8°; matrix = 256 × 172; voxel size = 1 mm^3 isotropic). The rs-fMRI data were acquired using a 2D EPI (TR = 2000 ms; TE = 30 ms; flip angle = 90°; matrix = 64 × 64; number of volumes = 180; and voxel size = 3.438 × 3.438 × 3.4 mm^3). The diffusion MRI data were acquired using a 2D EPI (TR = 8500 ms; TE = minimum; matrix = 128 × 128; voxel size = 1.875 × 1.875 × 2 mm^3; 61 directions; b-value = 1000 s/mm^2; and 1 number b0 image).

2.3. Data preprocessing

We preprocessed the T1-weighted data using FreeSurfer version 6.0 (Dale et al., 1999; Fischl, 2012; Fischl et al., 2001, 1999a, 1999b; Ségonne et al., 2007), which includes gradient nonuniformity correction, skull stripping, intensity normalization, and tissue segmentation. White and pial surfaces were generated through triangular surface tessellation, topology correction, inflation, and spherical registration to the fsaverage template surface. The rs-fMRI data were previously processed using C-PAC (https://fcp-indi.github.io) (Craddock et al., 2013), and provided by the ABIDE database (http://preprocessed-connectomes-project.org/abide/). The pipeline included slice timing and head motion correction, skull stripping, and intensity normalization. Nuisance variables of head motion, average white matter and cerebrospinal fluid signal, and linear/quadratic trends were removed using CompCor (Behzadi et al., 2007). Band-pass filtering between 0.01 and 0.1 Hz was applied, and rs-fMRI data were co-registered to T1-weighted data in MNI152 standard space with boundary-based rigid-body and nonlinear transformations. The rs-fMRI data were mapped to subject-specific midthickness surfaces and resampled to Conte69. Finally, surface-based spatial smoothing with a full-width-at-half-maximum of 5 mm was applied. The diffusion MRI data were processed using Mrtrix3 (Tournier et al., 2019), including correction for susceptibility distortions, head motion, and eddy currents. Quality control involved visual inspection of T1-weighted data, and cases with faulty cortical segmentation were excluded. Cases with an rs-fMRI data framewise displacement >0.3 mm were also excluded (Power et al., 2014; Power et al., 2012).

2.4. Structural and functional connectivity

Structural connectomes were generated from preprocessed diffusion MRI data using Mrtrix3 (Tournier et al., 2019). Anatomical constrained tractography was performed using different tissue types derived from the T1-weighted image, including cortical and subcortical grey matter, white matter, and cerebrospinal fluid (Smith et al., 2012). The T1-weighted MRI was registered to the diffusion MRI data with boundary-based registration, and the transformation was applied to different tissue types to register them onto the native diffusion MRI space. Multi-shell and multi-tissue response functions were estimated (Christiaens et al., 2015), and constrained spherical deconvolution and intensity normalization were performed (Jeurissen et al., 2014). Seeding from all white matter voxels, the tractogram was generated based on a probabilistic approach (Tournier et al., 2010, 2019; Power et al., 2012) with 40 million streamlines, with a maximum tract length of 250 and a fractional anisotropy cutoff of 0.06. Subsequently, spherical-deconvolution informed filtering of tractograms (SIFT2) was applied to reconstruct whole-brain streamlines weighted by the cross-section multipliers, which considers the fiber bundle's total intra-axonal space across its full cross-sectional extent (Smith et al., 2015). The structural connectome was built by mapping the reconstructed cross-section streamlines onto the Schaefer atlas with 200 parcels (Schaefer et al., 2018), then log-transformed to adjust for the scale (Fornito et al., 2016). Functional connectivity matrices were generated by calculating Pearson's correlations of time series between two different brain regions defined using the Schaefer atlas with 200 parcels (Schaefer et al., 2018), and the correlation coefficients were Fisher's r-to-z transformation to render data more normally distributed (Thompson and Fransson, 2016).

2.5. Functional connectivity prediction using structural connectivity

To predict functional connectivity from structural connectivity, we opted for a recently introduced Riemannian optimization approach (Benkarim et al., 2022). Core to this approach is the application of diffusion map embedding, a nonlinear dimensionality technique (Coifman and Lafon, 2006), to the structural connectivity matrix to generate low-dimensional eigenvectors (*i.e.,* diffusion maps), which are defined as follows:

$$\Psi_t(i) = (\lambda_0\psi_0(i),\ \lambda_1\psi_1(i), \ldots)^T, \tag{1}$$

where $\Psi_t(i)$ denotes the diffusion maps of a region i at diffusion time t, which controls the scale of eigenvalues, λ_k and ψ_k are the eigenvalues and eigenvectors, and T stands for transpose. Diffusion map embedding projects the original data into a low-dimensional eigenspace where distances between regions are related to their similarity in connectivity. The Euclidean distance among data points in the eigenspace is referred to as the diffusion distance, and it is defined as follows:

$$D_t^2(i,j) = \sum_{k\geq 0}\lambda_k^{2t}(\psi(i) - \psi(j))^2 = ||\Psi_t(i) - \Psi_t(j)||^2, \tag{2}$$

where $D_t^2(i,j)$ is the diffusion distance of the edge connecting the ith and jth brain region at diffusion time t, and $||\cdot||$ denotes the l_2-norm. Thus, data points (*i.e.,* brain regions) in the eigenspace are more closely located when longer diffusion times are applied. Here, we calculated the diffusion distances between the points across varying diffusion times. To predict functional connectivity, this approach uses kernel fusion to find a weighted combination of the kernels derived from the diffusion maps at each diffusion time using a radial basis function as follows:

$$\underset{\alpha\in R^m}{argmin}\left|\left|F - \sum_{t=1}^{m}\alpha_t K_t\right|\right|_F^2 + \mu_1||\alpha||_2^2,\ s.t.\ \alpha_t \geq 0,\ \forall t = 1, \ldots, m, \tag{3}$$

where F is the functional connectivity matrix, $K_t(i,j)$ is the kernel of a radial basis function that is defined as $\exp(-\gamma D_t^2(i,j))$, where γ is the kernel bandwidth, m is the total number of diffusion times, $\alpha_t \geq 0$ is the coefficient corresponding to the kernel, μ_1 is a trade-off parameter, and $\|\cdot\|_F$ is the Frobenius norm. The approach further uses a transformation matrix to rotate the diffusion maps before computing the kernels for each diffusion time so that the structural and functional embeddings share the same diffusion coordinates. Specifically, we aimed to find the rotation matrix Ω applied to the structural connectivity Y at diffusion time t as follows:

$$arg\ \underset{\substack{\Omega\in R^{n\times m}\\ \alpha\in R^m}}{min}\left|\left|F - \sum_{t=1}^{m}\alpha_t k(\Omega Y_t)\right|\right|_F^2 + \mu_1||\alpha||_2^2,$$

$$\begin{aligned} s.t.\ \Omega\Omega^T = \Omega^T\Omega = I_n, \\ \det(\Omega) = 1, \\ \alpha_t \geq 0, \\ \forall t = 1, \cdots, m, \end{aligned} \tag{4}$$

where I_n is the identity matrix with the size of $n \times n$, $\det(\cdot)$ is the matrix determinant, and $[k(\Gamma_t)]_{i,j} = \exp(-\gamma ||\Gamma_t(i) - \Gamma_t(j)||^2)$, where $\Gamma_t(i) = \Omega Y_t(i)$ is the rotated structural diffusion map of the ith brain region. The rotation matrix may help identify the optimal paths through which to propagate information between different brain regions. Here, to solve the optimization problem, the Riemannian conjugate gradient algorithm (Absil et al., 2008) implemented in the Pymanopt toolbox (Townsend et al., 2016) was used. Details can be found elsewhere (Benkarim et al., 2022). We performed the prediction procedure for ASD and control groups separately with a five-fold cross-validation. The prediction performance was assessed by calculating Pearson's correlation of the upper triangular elements between empirical and predicted functional connectivity matrices. We assessed the prediction accuracy with varying diffusion times between $t = 1$ and $t = 10$. Differences in prediction accuracy between ASD and control groups were assessed based on 1000 permutation tests. We randomly assigned subject indices and calculated differences in prediction accuracy between the new groups (Δr) to construct a null distribution. If the real difference did not belong to 95% of the null distribution, it was deemed significant.

2.6. Between-group differences in regional prediction accuracy across diffusion times

We also assessed regional prediction performances across varying diffusion times. We specifically investigated whether changes in structure-function coupling differed between ASD and neurotypicals. Our framework leveraged a Riemannian manifold prediction across diffusion times in a global and region-specific manner to assess the impact of polysynaptic communication. For each diffusion time, we calculated Pearson's correlations between the empirical and predicted functional connectivity matrix of each brain region. In addition, at diffusion times that showed significant between-group differences in global prediction accuracy, we compared the regional prediction performance between ASD and control groups while controlling for age, sex, and site using a general linear model implemented in SurfStat (Larivière et al., 2023; Worsley et al., 2009). We corrected for multiple comparisons across regions using false discovery rate (FDR) adjustment (Benjamini and Hochberg, 1995). To assess the improvement of the prediction accuracy across diffusion times, we calculated the difference in prediction accuracy between the highest ($t = 10$) and lowest ($t = 1$) diffusion times (*i.e.,* Δprediction accuracy). We then compared the Δprediction accuracy between ASD and control groups with controlling for age, sex, and site using a general linear model implemented in SurfStat (Larivière et al., 2023; Worsley et al., 2009), and multiple comparisons across brain regions were corrected using FDR (Benjamini and Hochberg, 1995).

2.7. Topological and network organization of prediction accuracy difference across diffusion times

We assessed underlying connectome profiles of the across-diffusion time prediction accuracy difference. First, we z-scored values in all participants relative to the distribution in neurotypicals. In other words, we removed the mean from neurotypicals from all values and divided the result by the standard deviation in neurotypicals. This procedure, thus, scaled individual values relative to the distribution of controls. We then stratified the parcel-wise Δprediction accuracy according to seven functional communities (visual, somatomotor, dorsal attention, ventral attention, limbic, frontoparietal, default mode) (Yeo et al., 2011) and four cortical hierarchical levels (idiotypic, unimodal association, heteromodal association, paralimbic) (Mesulam, 1998). For each macroscale functional network or level of cortical hierarchy, we quantitatively assessed between-group differences in prediction accuracy improvements using two-sample t-tests. The significance of the differences was assessed using 1000 permutation tests by randomly assigning subject indices, and multiple comparisons across brain networks or hierarchies were corrected using the FDR procedure (Benjamini and Hochberg, 1995). Next, we associated Δprediction accuracy with a functional principal gradient, representing a cortical hierarchy running from low-level sensory to higher-order transmodal system (Margulies et al., 2016). We obtained the functional gradient from the BrainSpace toolbox (Vos de Wael et al., 2020), which was generated using the Human Connectome Project database (Van Essen et al., 2013). Specifically, an affinity matrix was constructed with a normalized angle kernel with the top 10% entries for each parcel, and diffusion map embedding was applied (Coifman and Lafon, 2006), which is robust to noise and computationally efficient compared to other nonlinear manifold learning techniques (Tenenbaum et al., 2000; von Luxburg, 2007). It is controlled by two parameters α and t, where α controls the influence of the density of sampling points on the manifold ($\alpha = 0$, maximal influence; $\alpha = 1$, no influence) and t scales the eigenvalues of the diffusion operator. The parameters were set as $\alpha = 0.5$ and $t = 0$ to retain the global relations between data points in the embedded space following prior applications (Hong et al., 2019b; Margulies et al., 2016; Paquola et al., 2019; Park et al., 2021d; Vos de Wael et al., 2020). In datasets in both healthy adults as well as typically developing individuals (Leech et al., 2023; Smallwood et al., 2021; Valk et al., 2022), the gradient has previously been shown to follow established models of the primate cortical functional hierarchy and specifically differentiates sensory and motor networks from transmodal systems such as the default-mode network. We then associated the functional gradient with Δprediction accuracy of each individual within each group. The significance of the correlation was determined using 1000 non-parametric spin-tests for accounting for spatial autocorrelation (Alexander-Bloch et al., 2018; Larivière et al., 2021; Markello and Misic, 2021). Between-group differences in the associations between ASD and control groups were assessed using two-sample t-tests with 1000 permutation tests.

2.8. Associations with behavioral phenotypes

As a final analysis, we investigated behavioral associations of diffusion time-related structure-function coupling. We performed multivariate analysis using partial least squares (PLS) (Krishnan et al., 2011; McIntosh and Mišić, 2013) to associate Δprediction accuracy across diffusion times with ADOS social cognition, communication, and repetitive behavior scores (Lord et al., 2000) as well as verbal and performance intelligence quotient (IQ) and their ratio (verbal/performance IQ) (Hong et al., 2022). PLS is an unsupervised multivariate statistical technique that decomposes two datasets into orthogonal sets of latent variables with maximum covariance (Krishnan et al., 2011; McIntosh and Mišić, 2013). We performed PLS analysis with 1000 bootstraps by randomly selecting subjects and estimated PLS scores as well as loadings of the latent variables. We calculated Pearson's correlation between the PLS scores of Δprediction accuracy and behavioral phenotypes to assess the strength of their associations. The contribution of the features of brain regions and/or behavioral phenotypes was quantified using PLS loadings. Specifically, we calculated a bootstrap ratio by dividing the mean loadings by standard errors (Zeighami et al., 2019). We thresholded the bootstrap ratio with a 95% confidence interval (Zeighami et al., 2019).

2.9. Sensitivity analysis

a) Parcellation schemes. Our main analysis interrogated structure-function coupling using the Schaefer atlas with 200 parcels (Schaefer et al., 2018). To assess robustness across different spatial scales, we also

predicted functional connectivity from structural connectivity based on Schaefer atlases with either 100 or 300 parcels.

b) Only male participants. As our dataset contained a large imbalance of male compared to female participants, we performed an analogous analysis using only male participants.

c) Site effects. We obtained the data from three different sites. To assess the consistency of the results across different sites, we performed the structure-function coupling analysis for each site.

3. Results

3.1. Global imbalances in structure-function coupling in ASD

Based on connectome manifold models (Benkarim et al., 2022), we simulated resting-state functional connectivity among 200 cortical regions (Schaefer et al., 2018) from tractography-derived structural connectivity data (Benkarim et al., 2022). In brief, the technique *(i)* applies nonlinear dimensionality reduction (*i.e.,* diffusion map embedding) (Coifman and Lafon, 2006; Vos de Wael et al., 2020) to a structural connectome, *(ii)* varies the diffusion time parameter t of the embedding technique to simulate connectivity-guided random walks (Fig. 1A), and *(iii)* the kernels derived from the corresponding diffusion times using a radial basis function are fused to minimize the difference between the actual functional connectivity and diffusion maps applied. Before generating the kernels, the algorithm uses a transformation matrix to rotate diffusion maps to find optimal paths through which to propagate information between different brain regions at each diffusion time. Structure-function coupling at the global level was quantified as the linear correlation of the upper triangular elements between empirical and simulated functional connectivity matrices across diffusion times t (from $t = 1$ to $t = 10$, with higher t indicating an increased contribution of polysynaptic communication across indirect paths; Fig. 1B). In both neurotypicals and ASD, coupling monotonically increased with higher diffusion times. Notably, controls showed globally higher prediction performance between t = 2–4. We quantitatively assessed between-group differences in coupling using 1000 permutation tests by shuffling subject indices and confirmed higher performance in controls relative to ASD between $t = 2$ and $t = 4$ ($p_{perm} = 0.020, 0.044, 0.038$; Fig. 1C). The results indicate that both controls and ASD displayed an influence of polysynaptic communication on structure-function coupling, and stronger global coupling in controls than in ASD.

3.2. Regional structure-function imbalances

We assessed regional prediction performance gains across variable diffusion times t to explore the contribution of polysynaptic communication on the prediction of brain function. For both controls and ASD, sensory/motor areas showed higher prediction accuracy at low diffusion times compared to transmodal systems (*i.e.,* default-mode network and paralimbic cortices). With increasing diffusion times, regional prediction performance increased in both groups, with higher performance in controls (Fig. 2A). When comparing the regional prediction accuracy between the ASD and control groups, we found consistent decreases in prediction accuracy in orbitofrontal and precentral regions in the ASD group, while consistent increases were observed in centro-opercular regions (**Supplementary Fig. 1**). To assess differences in prediction accuracy across diffusion times, we calculated prediction accuracy differences between $t = 10$ and $t = 1$ (Δprediction accuracy) in both cohorts separately (Fig. 2B). We observed marked differences in transmodal compared to sensory/motor systems, and these differences were overall larger in controls than ASD (FDR < 0.05). Prediction accuracy differences were consistent when we assessed differences between the high diffusion times (t = 4∼9) and the lowest diffusion time ($t = 1$) (**Supplementary Fig. 2**).

3.3. Topographic associations to structure-function imbalances

We stratified findings with respect to established taxonomies of intrinsic functional organization. First, we assessed across-diffusion time differences in structure-function prediction performance (Δprediction accuracy) across seven intrinsic functional networks (Yeo et al., 2011) or levels of the primate cortical hierarchy (Mesulam, 1998) (Fig. 3A). We noted overall smaller improvement in the default-mode network in ASD relative to controls, while visual and limbic networks showed increased improvement. Second, we explored associations with the principal functional gradient, which discriminates sensory/visual from transmodal systems in a continuous manner based on data-driven connectome analysis. The first principal functional gradient was estimated from resting-state functional connectivity obtained from the Human Connectome Project database (Van Essen et al., 2013), using the BrainSpace toolbox version 0.1.10 (https://github.com/MICA-MNI/BrainSpace) (Coifman and Lafon, 2006; Vos de Wael et al., 2020) (Fig. 3B). We observed significant correlations with the functional gradient, even after accounting for spatial autocorrelation, in both groups (control: $r = 0.472 \pm 0.218$, $p_{spin} = 0.015$; ASD: $r = 0.323 \pm 0.201$, $p_{spin} = 0.023$; Fig. 3B). Similar findings were observed when we fitted Δprediction accuracy to the functional gradient using a quadratic function, which showed slight improvements in fit (**Supplementary Fig. 3**). In both the linear and quadratic cases, associations were significantly different between groups and stronger in controls (two-sample t-tests with 1000 permutations $p < 0.001$; Fig. 3B and **Supplementary Fig. 3**).

3.4. Associations with behavioral phenotypes

We studied associations between Δprediction accuracy and behavioral phenotypes of ADOS scores (social cognition, communication, and repetitive behavior) as well as verbal and non-verbal IQ and their ratio (verbal/non-verbal IQ) (Hong et al., 2022) using PLS analyses (Krishnan et al., 2011; McIntosh and Mišić, 2013). We performed the PLS analysis with 1000 bootstraps, and the first latent variable explained 33.4% of covariance between Δprediction accuracy and behavioral phenotypes (Fig. 4A). The estimated PLS scores showed significant correlations across bootstraps ($r = 0.426 \pm 0.093$, $p_{perm} = 0.010$; Fig. 4B). We assessed the contribution of these features using bootstrap ratio calculated based on the loadings (Zeighami et al., 2019). We found that Δprediction accuracy in sensory and frontoparietal regions was associated with lower social cognition and communication-related autistic symptoms and IQ ratio, indicating less autistic characteristics (Fig. 4C). On the other hand, Δprediction accuracy in temporal and limbic regions was associated with higher autistic symptom, particularly, repetitive behaviors (**Supplementary Fig. 4**).

3.5. Sensitivity analyses

a) Parcellation schemes. Results were largely consistent with the original findings when using an alternative subdivision of the cortex into either 100 or 300 parcels (**Supplementary Figs. 5–6**).

b) Only male participants. We additionally performed the same analyses using only male participants and found comparable results (**Supplementary Fig. 7**).

c) Site effects. We performed the analyses for each site separately. We found overall similar patterns but decreased effects, which may be due to the small sample size (**Supplementary Figs. 8–10**).

4. Discussion

The correspondence of brain structure and function is a core tenet of neuroscience (Baum et al., 2020; Honey et al., 2009; Mišic et al., 2016; Paquola et al., 2019, 2020; Park et al., 2021d; Snyder and Bauer, 2019; Suárez et al., 2020; Vázquez-Rodríguez et al., 2019), and the advent of

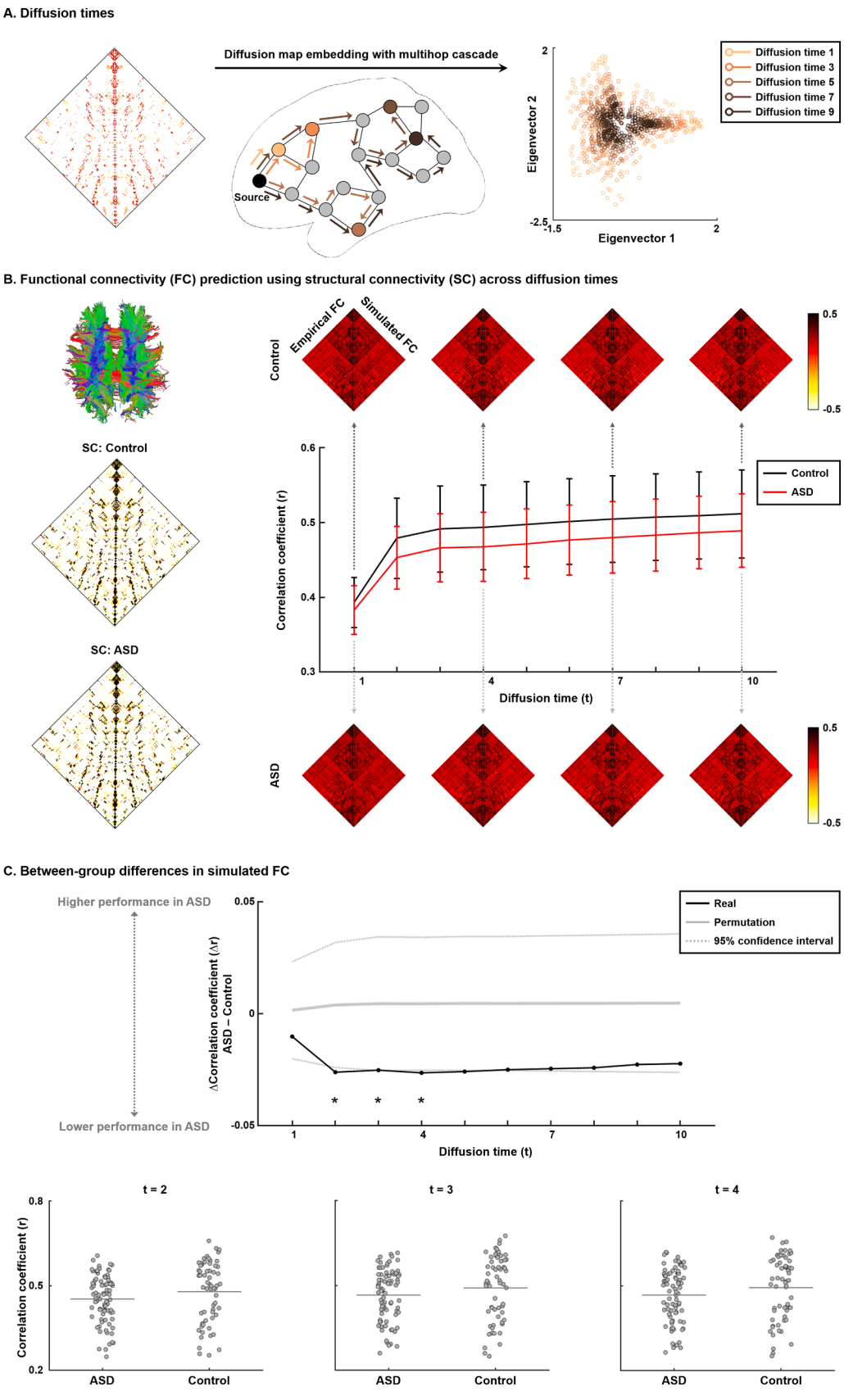

(caption on next page)

Fig. 1. Global imbalances in structure-function coupling in ASD. **(A)** Schema of the Riemannian manifold optimization approach that was used to simulate functional connectivity (FC) along a structural connectome (SC) as a function of diffusion time *t*. This approach projects SC (left) onto the low-dimensional latent space (right) with different diffusion times that indicate multihop processes (middle) using a diffusion map embedding algorithm. **(B)** Group-level SC matrices in controls and ASD (left). Correlation coefficients between empirical and simulated FC in controls (black) and ASD (red) as a function of *t* (right). Error bars represent the SD across individuals. Shown are empirical (left) and simulated FC (right) matrices across four representative diffusion times ($t = 1$, 4, 7, and 10). **(C)** Between-group differences in prediction performance between controls and ASD (upper panel). A black line indicates real differences in prediction performance between groups, a solid gray line indicates mean prediction accuracy differences across 1000 permutation tests, and dotted gray lines indicate the 95% confidence interval. Significant between-group differences are reported with asterisks. Shown are correlation coefficients between an individual's empirical and simulated FC for those diffusion times that showed significant between-group differences (lower panels). *Abbreviations:* ASD, autism spectrum disorder; SD, standard deviation.

multimodal imaging and connectomics methods have culminated in efforts to predict large-scale brain function and inter-regional functional interactions from representations of brain wiring in healthy humans (Benkarim et al., 2022; Damoiseaux and Greicius, 2009; Goñi et al., 2014; Honey et al., 2009; Seguin et al., 2019; Suárez et al., 2020). Here, we utilized unsupervised connectivity manifold learning and alignment techniques to index structure-function coupling in ASD, a common neurodevelopmental indication increasingly conceptualized as a connectopathy, and explore the role of polysynaptic communication mechanisms on structure-function coupling. Studying individuals with ASD and neurotypical controls, we observed structure-function coupling in both groups to be overall high and generally increasing when additionally incorporating polysynaptic communication in the modelling, particularly in transmodal systems that have been more challenging to model in prior studies (Benkarim et al., 2022; Suárez et al., 2020; Vázquez-Rodríguez et al., 2019). On the other hand, compared to controls, ASD showed imbalanced and overall lower structure-function coupling. These reductions were particularly observed in polysynaptic regimes and transmodal regions. Structure-function coupling imbalances in ASD were also aligned with prototypical and data-driven descriptions of the primate cortical hierarchy, indicating a sensory-to-transmodal gradient of alterations in structure-function coupling in ASD. Findings reflected autism symptoms and imbalances in verbal/non-verbal intelligence dimensions. Collectively, our findings show hierarchy-dependent imbalances in structurally-governed network communication in ASD and may offer a novel and behaviorally relevant perspective of autism connectopathy.

Our work investigated connectome-level structure-function coupling using a Riemannian manifold optimization procedure (Benkarim et al., 2022). In a recent study in neurotypical adults, this approach provided a faithful individual participant-level prediction of intrinsic functional interactions based on structural connectomes (Benkarim et al., 2022). It can be tuned across diffusion time parameters, interpretable as an increasing influence of polysynaptic structure-function coupling mechanisms. Comparing prediction accuracy between neurotypicals and ASD, our findings revealed globally reduced coupling in the latter. Coupling was particularly reduced towards higher diffusion times, and ASD-related reductions were most marked in transmodal systems such as the default mode and frontoparietal networks. Such findings indicate a hierarchy-dependent alteration in structure-function coupling in ASD, particularly in polysynaptic subnetworks. These findings suggest that links between brain structure and function are not as straightforward in ASD compared to controls, which may relate to several previously identified factors. Neuroimaging studies have shown atypical cortical morphology and microstructure, aberrant white matter fiber architecture, and reorganized structural network topology in ASD (Cai et al., 2022; Hong et al., 2018; Hong et al., 2019b). Despite only a little work assessing links between structural alterations and atypical function in ASD, studies have indicated atypical functional connectivity between different brain areas (Di Martino et al., 2014; Hull et al., 2017; Müller et al., 2011). Moreover, several reports emphasized increased spatial shifting of functional network layout in ASD, a finding also referred to as idiosyncrasy (Benkarim et al., 2021; Dickie et al., 2018; Hahamy et al., 2015; Uddin et al., 2015), alongside findings suggesting increased signal variation in this cohort (Takahashi et al., 2016). These factors may collectively result in lower predictability of functional signaling and interactions from structural connectivity information and hence contribute to the observed findings in this study.

Brain hierarchy along the sensory/motor-association axis underpins primate cortical organization, initially inferred from invasive *post-mortem* findings in non-human animals (Mesulam, 1998). Recently, our understanding of the cortical hierarchical organization has been solidified with human neuroimaging, notably functional connectivity research (Bethlehem et al., 2020; Margulies et al., 2016; Mckeown et al., 2020; Murphy et al., 2019; Park et al., 2021c), microstructural profiling (Burt et al., 2018; Paquola et al., 2019), and tractography-derived structural connectomics (Kharabian Masouleh et al., 2020; Park et al., 2021a, 2021b). In our study, inter-regional variations in structure-function prediction performance followed dimensional and clustering-based approximations of the cortical functional hierarchy. In particular, we observed lower structure-function coupling towards transmodal systems when incorporating monosynaptic mechanisms, which, however, increased with larger diffusion times and hence, polysynaptic communication. Overall reduced structure-function coupling in transmodal systems compared to sensory/motor and unimodal networks echoes prior findings (Valk et al., 2022; Vázquez-Rodríguez et al., 2019), in particular when bare diffusion MRI tractography measures without explicit incorporation of polysynaptic communication inform the modeling strategy. Transmodal regions are known to increasingly engage in long-range and more centralized communication, underpinning integrative cognitive functions (Park et al., 2021d). In our work, performance reductions in ASD relative to neurotypicals are related mainly to reduced hierarchy-specific gains in predicting functions that would have otherwise resulted from the incorporation of polysynaptic communication in ASD. Previous work from our group and others based on functional and structural neuroimaging has suggested atypical connectome hierarchy, and suggested that densely integrated rich core nodes may assume a major role in this process (Hong et al., 2019b; Park et al., 2021b), possibly in lieu of their implication in multiple, polysynaptic communication pathways.

Multivariate associative techniques revealed that altered structure-function relations in ASD reflected behavioral symptoms and cognitive phenotypes, here indexed by the ADOS scale and verbal and non-verbal intelligence dimensions. It should be noted that our results were derived from small samples and assessed using four-fold cross-validation only, requiring validations in larger samples with multimodal imaging data to assess generalizability. Findings, nevertheless, suggested a broad implication of different brain systems, notably transmodal systems, such as the default-mode network. These systems have been shown to contribute to both typical and atypical social interaction and communication, and higher cognitive processes more generally (Assaf et al., 2010; Mars et al., 2012; Padmanabhan et al., 2017; Paquola et al., 2022; Raichle, 2015; Smallwood et al., 2021). Moreover, systems at the apex of the putative cortical hierarchy undergo ongoing maturational processes in typical childhood and adolescence, which shift networks towards a more clustered layout and progressively differentiate these from other macroscale networks, possibly due to the strengthening of long-range connections (Baum et al., 2020; Fan et al., 2021; Park et al., 2022). Our findings suggest that atypical polysynaptic communication in higher-order transmodal areas, in part, reflects those symptoms and could serve as a potential diagnostic marker of affected individuals.

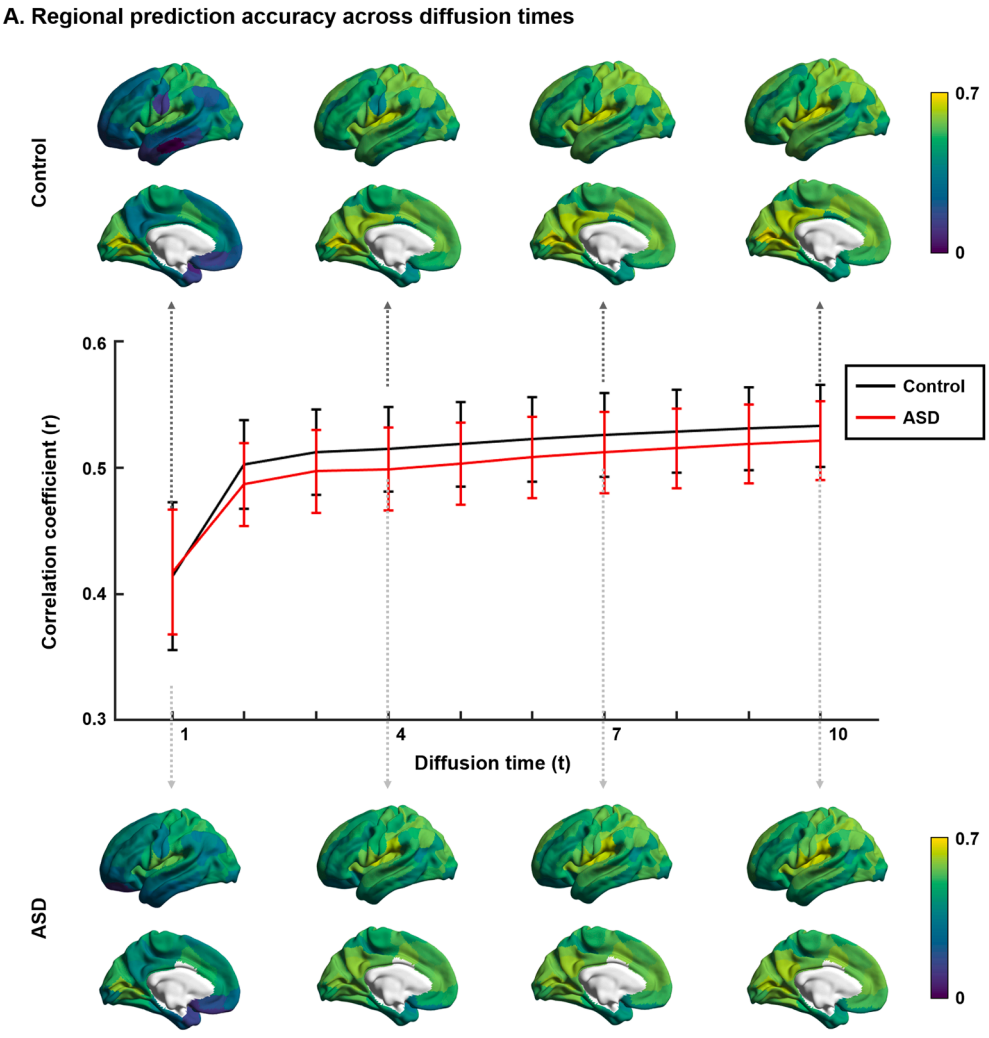

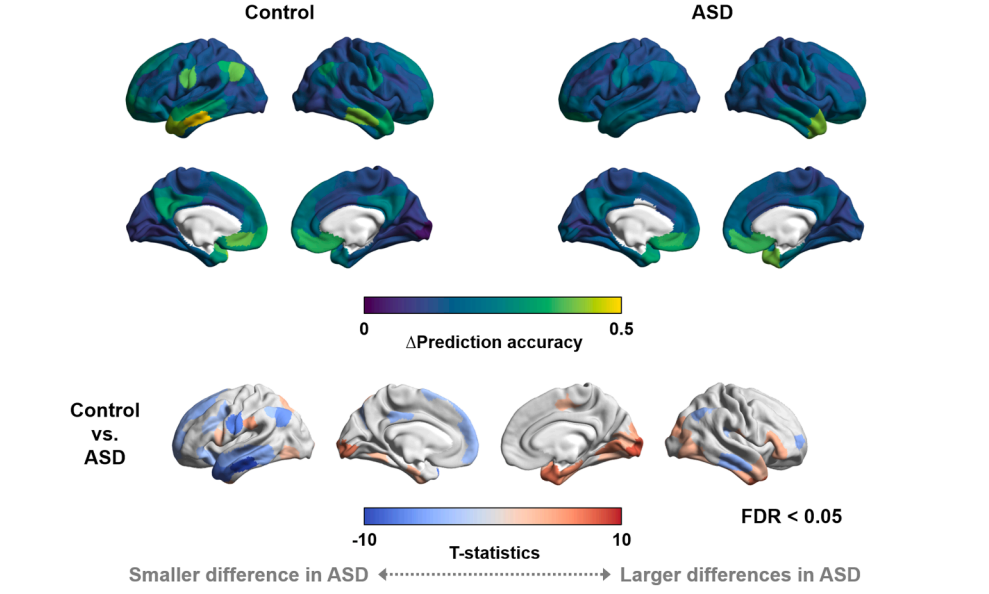

(caption on next page)

Fig. 2. Regional structure-function imbalances. **(A)** Correlation coefficients between empirical and simulated functional connectivity (FC) across different diffusion times t are shown on brain surfaces for control and ASD groups. The plot indicates correlation coefficients between the empirical and simulated FC in controls (black) and ASD (red) as a function of diffusion time. Error bars represent the SD across brain regions. **(B)** Shown are differences in prediction accuracy between the highest ($t = 10$) and lowest ($t = 1$) diffusion times (Δprediction accuracy) for both groups (upper panels). We assessed between-group differences in Δprediction accuracy between controls and ASDs (lower panel). *Abbreviations:* ASD, autism spectrum disorder; SD, standard deviation; FDR, false discovery rate.

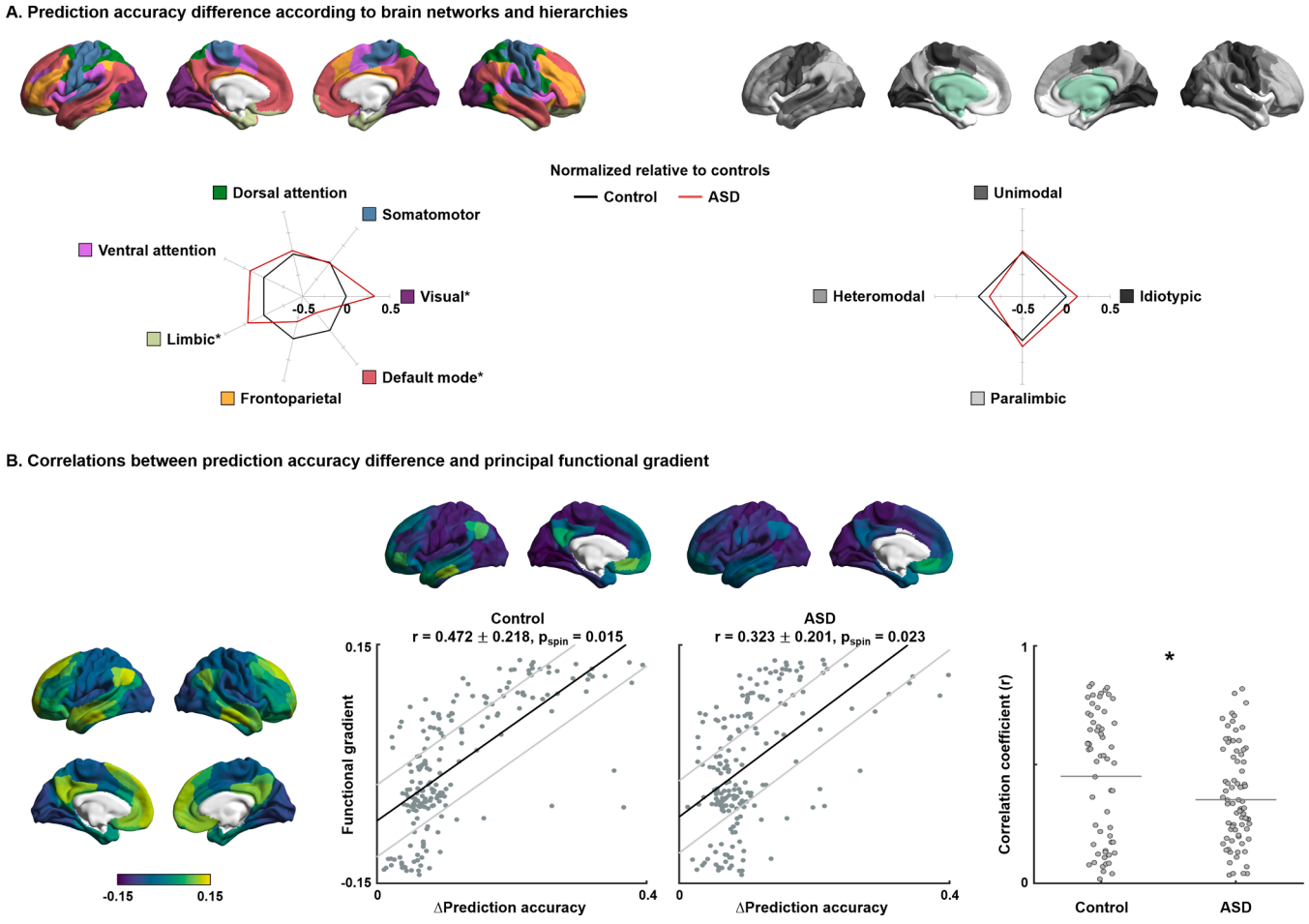

Fig. 3. Topographic associations. **(A)** We stratified the prediction accuracy difference between diffusion time $t = 10$ and $t = 1$ (Δprediction accuracy) according to functional communities (left) (Yeo et al., 2011) and cortical hierarchies (right) (Mesulam, 1998). Spider plots show normalized Δprediction accuracy, where the values of ASD are normalized relative to controls. Asterisks indicate the brain network or cortical hierarchy that showed significant between-group differences. **(B)** The principal functional gradient is visualized on brain surfaces (left). We calculated linear correlations between the gradient and Δprediction accuracy for both controls and ASD individuals, where gray lines indicate SD across individuals (center). In the right panel, one can see the correlation coefficients of each individual in both groups, where the asterisk indicates a significant difference. *Abbreviations:* ASD, autism spectrum disorder; SD, standard deviation.

5. Code availability

The codes for simulating functional connectivity from structural connectivity are available at https://github.com/MICA-MNI/micaopen/tree/master/sf_prediction; codes for gradient generation are available at https://github.com/MICA-MNI/BrainSpace; codes for graph measures calculation are available at https://sites.google.com/site/bctnet/.

CRediT authorship contribution statement

Bo-yong Park: Conceptualization, Data curation, Formal analysis, Funding acquisition, Investigation, Methodology, Software, Resources, Validation, Visualization, Writing – original draft. **Oualid Benkarim:** Formal analysis, Methodology, Resources, Software, Writing – review & editing. **Clara F. Weber:** Validation, Writing – review & editing. **Valeria Kebets:** Conceptualization, Methodology, Writing – review & editing. **Serena Fett:** Writing – review & editing. **Seulki Yoo:** Writing – review & editing. **Adriana Di Martino:** Conceptualization, Data curation, Writing – review & editing. **Michael P. Milham:** Conceptualization, Data curation, Writing – review & editing. **Bratislav Misic:** Methodology, Software, Writing – review & editing. **Sofie L. Valk:** . **Seok-Jun Hong:** Conceptualization, Methodology, Writing – review & editing. **Boris C. Bernhardt:** Conceptualization, Data curation, Formal analysis, Funding acquisition, Investigation, Methodology, Project administration, Resources, Software, Supervision, Validation, Visualization, Writing – original draft.

Declaration of Competing Interest

All authors declare no conflicts of interest.

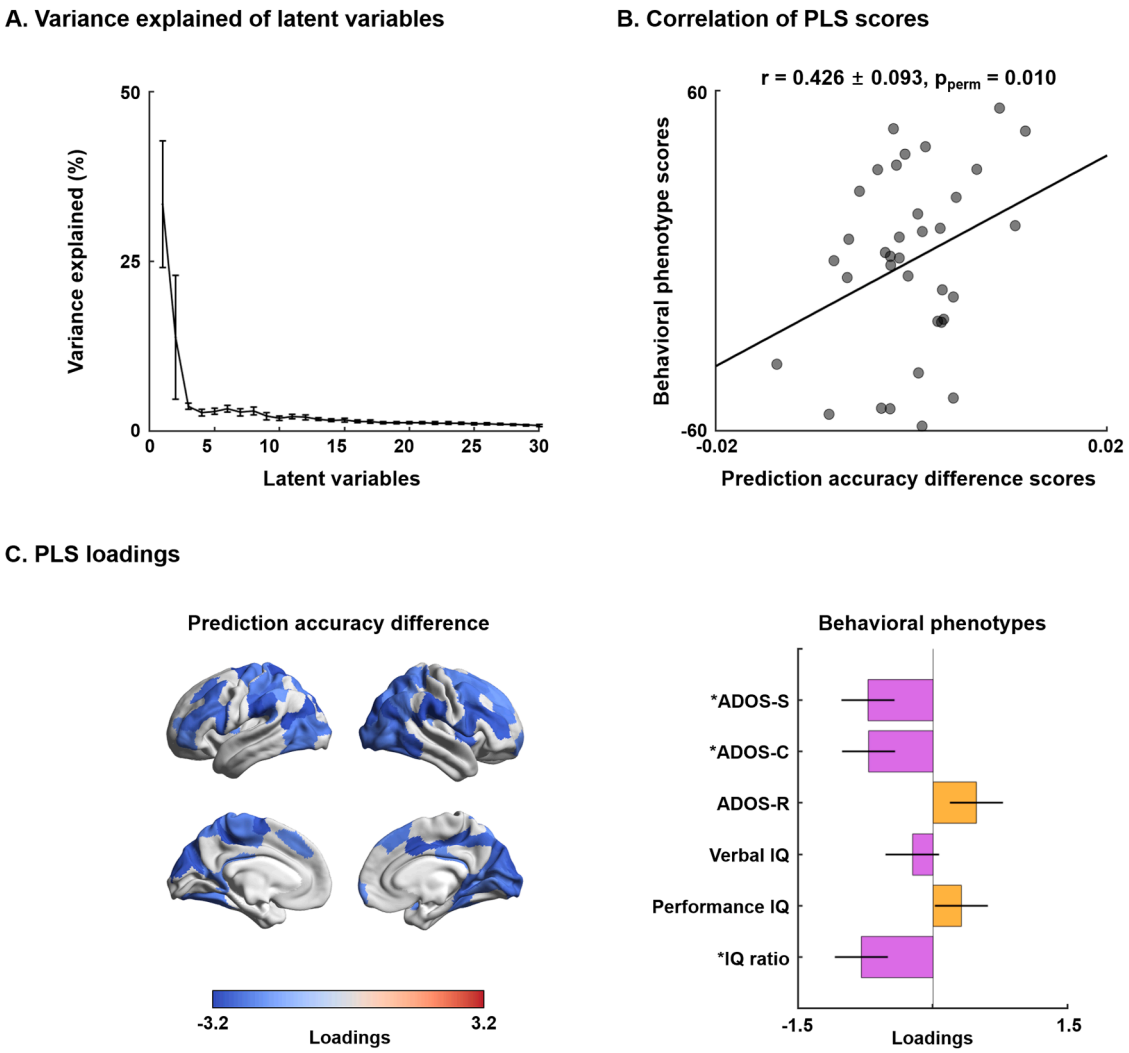

Fig. 4. Multivariate associations between structure-function coupling imbalances and behavioral phenotypes of ASD. **(A)** The scree plot shows the percent variance explained by each latent variable, where the error bars indicate SD across bootstraps. **(B)** We calculated linear correlations between PLS scores of Δprediction accuracy and behavioral phenotypes of the first latent variable in ASD, which explained almost 33.4% of the variance. **(C)** Shown are PLS loading-based bootstrap ratios of Δprediction accuracy (*left*) and behavioral phenotypes (*right*). Brain regions and behavioral phenotypes that showed significance are shown and marked with asterisks. *Abbreviations*: SD, standard deviation; PLS, partial least squares; ADOS-S, Autism Diagnostic Observation Schedule – social cognition; ADOS-C, Autism Diagnostic Observation Schedule – communication; ADOS-R, Autism Diagnostic Observation Schedule – repeated behavior; IQ, intelligence quotient.

Data availability

I have shared the link to my data/code at the Attach File step

Funding

Bo-yong Park was funded by the National Research Foundation of Korea (NRF-2021R1F1A1052303; NRF-2022R1A5A7033499), Institute for Information and Communications Technology Planning and Evaluation (IITP) funded by the Korea Government (MSIT) (No. 2022–0–00448, Deep Total Recall: Continual Learning for Human-Like Recall of Artificial Neural Networks; No. RS-2022–00155915, Artificial Intelligence Convergence Innovation Human Resources Development (Inha University); No. 2021–0–02068, Artificial Intelligence Innovation Hub), and Institute for Basic Science (IBS-R015-D1). Boris C. Bernhardt acknowledges research support from the National Science and Engineering Research Council of Canada (NSERC Discovery-1304413), the CIHR (FDN-154298, PJT), SickKids Foundation (NI17–039), Azrieli Center for Autism Research (ACAR-TACC), BrainCanada (Future Leaders), Fonds de la Recherche du Québec – Santé (FRQ-S), the Tier-2 Canada Research Chairs program, Helmholtz Association's Initiative and Networking Fund under the Helmholtz International Lab grant agreement InterLabs-0015, and the Canada First Research Excellence Fund (CFREF Competition 2, 2015–2016) awarded to the Healthy Brains, Healthy Lives initiative at McGill University, through the Helmholtz International BigBrain Analytics and Learning Laboratory (HIBALL).

Supplementary materials

Supplementary material associated with this article can be found, in the online version, at doi:10.1016/j.neuroimage.2023.120481.

References

Absil, P.A., Mahony, R., Sepulchre, R., 2008. Optimization Algorithms on Matrix Manifolds. Princeton University Press. https://doi.org/10.1515/9781400830244.

Alexander-Bloch, A.F., Shou, H., Liu, S., Satterthwaite, T.D., Glahn, D.C., Shinohara, R.T., Vandekar, S.N., Raznahan, A., 2018. On testing for spatial correspondence between maps of human brain structure and function. Neuroimage 178, 540–551. https://doi.org/10.1016/j.neuroimage.2018.05.070.

Amaral, D.G., Schumann, C.M., Nordahl, C.W., 2008. Neuroanatomy of autism. Trends Neurosci. 31, 137–145. https://doi.org/10.1016/j.tins.2007.12.005.

Assaf, M., Jagannathan, K., Calhoun, V.D., Miller, L., Stevens, M.C., Sahl, R., O'Boyle, J. G., Schultz, R.T., Pearlson, G.D., 2010. Abnormal functional connectivity of default mode sub-networks in autism spectrum disorder patients. Neuroimage 53, 247–256. https://doi.org/10.1016/j.neuroimage.2010.05.067.

Avena-Koenigsberger, A., Misic, B., Sporns, O., 2018. Communication dynamics in complex brain networks. Nat. Rev. Neurosci. 19, 17–33. https://doi.org/10.1038/nrn.2017.149.

Avena-Koenigsberger, A., Yan, X., Kolchinsky, A., Van Den Heuvel, M.P., Hagmann, P., Sporns, O., 2019. A spectrum of routing strategies for brain networks. PLoS Comput. Biol. 15, 1–24. https://doi.org/10.1371/journal.pcbi.1006833.

Baum, G.L., Cui, Z., Roalf, D.R., Ciric, R., Betzel, R.F., Larsen, B., Cieslak, M., Cook, P.A., Xia, C.H., Moore, T.M., Ruparel, K., Oathes, D.J., Alexander-Bloch, A.F., Shinohara, R.T., Raznahan, A., Gur, R.E., Gur, R.C., Bassett, D.S., Satterthwaite, T.D., 2020. Development of structure–function coupling in human brain networks during youth. Proc. Natl. Acad. Sci. U.S.A. 117, 771–778. https://doi.org/10.1073/pnas.1912034117.

Bazinet, V., Vos de Wael, R., Hagmann, P., Bernhardt, B.C., Misic, B., 2021. Multiscale communication in cortico-cortical networks. Neuroimage 243, 118546. https://doi.org/10.1016/j.neuroimage.2021.118546.

Becker, C.O., Pequito, S., Pappas, G.J., Miller, M.B., Grafton, S.T., Bassett, D.S., Preciado, V.M., 2018. Spectral mapping of brain functional connectivity from diffusion imaging. Sci. Rep. 8 https://doi.org/10.1038/s41598-017-18769-x, 1411.

Behzadi, Y., Restom, K., Liau, J., Liu, T.T., 2007. A component based noise correction method (CompCor) for BOLD and perfusion based fMRI. Neuroimage 37, 90–101. https://doi.org/10.1016/j.neuroimage.2007.04.042.

Benjamini, Y., Hochberg, Y., 1995. Controlling the False Discovery Rate : A Practical and Powerful Approach to Multiple Testing. J. R. Stat. Soc. 57, 289–300.

Benkarim, O., Paquola, C., Park, B., Royer, J., Rodríguez-Cruces, R., Vos de Wael, R., Misic, B., Piella, G., Bernhardt, B.C., 2022. A Riemannian approach to predicting brain function from the structural connectome. Neuroimage 257, 119299. https://doi.org/10.1016/j.neuroimage.2022.119299.

Benkarim, O., Paquola, C., Park, B.yong, Hong, S.J., Royer, J., Vos de Wael, R., Lariviere, S., Valk, S., Bzdok, D., Mottron, L., C., Bernhardt, B., 2021. Connectivity alterations in autism reflect functional idiosyncrasy. Commun. Biol. 4, 1078. https://doi.org/10.1038/s42003-021-02572-6.

Bernhardt, B.C., Smallwood, J., Keilholz, S., Margulies, D.S., 2022. Gradients in brain organization. Neuroimage 251. https://doi.org/10.1016/j.neuroimage.2022.118987.

Bethlehem, R.A.I., Paquola, C., Seidlitz, J., Ronan, L., Bernhardt, B., Consortium, C.C.A. N., Tsvetanov, K.A., 2020. Dispersion of functional gradients across the adult lifespan. Neuroimage 222, 117299. https://doi.org/10.1016/j.neuroimage.2020.117299.

Breakspear, M., 2017. Dynamic models of large-scale brain activity. Nat. Neurosci. 20, 340–352. https://doi.org/10.1038/nn.4497.

Burt, J.B., Demirtaş, M., Eckner, W.J., Navejar, N.M., Ji, J.L., Martin, W.J., Bernacchia, A., Anticevic, A., Murray, J.D., 2018. Hierarchy of transcriptomic specialization across human cortex captured by structural neuroimaging topography. Nat. Neurosci. 21, 1251–1259. https://doi.org/10.1038/s41593-018-0195-0.

Cai, Y., Zhao, J., Wang, L., Xie, Y., Fan, X., 2022. Altered topological properties of white matter structural network in adults with autism spectrum disorder. Asian J. Psychiatr. 75, 103211 https://doi.org/10.1016/j.ajp.2022.103211.

Christensen, D.L., Braun, K.V.N., Baio, J., Bilder, D., Charles, J., Constantino, J.N., Daniels, J., Durkin, M.S., Fitzgerald, R.T., Kurzius-Spencer, M., Lee, L.C., Pettygrove, S., Robinson, C., Schulz, E., Wells, C., Wingate, M.S., Zahorodny, W., Yeargin-Allsopp, M., 2018. Prevalence and Characteristics of Autism Spectrum Disorder Among Children Aged 8 Years — Autism and Developmental Disabilities Monitoring Network, 11 Sites. United States, 2012 MMWR Surveill. Summ. 65, 1–23. https://doi.org/10.15585/mmwr.ss6513a1.

Christiaens, D., Reisert, M., Dhollander, T., Sunaert, S., Suetens, P., Maes, F., 2015. Global tractography of multi-shell diffusion-weighted imaging data using a multi-tissue model. Neuroimage 123, 89–101. https://doi.org/10.1016/j.neuroimage.2015.08.008.

Coifman, R.R., Lafon, S., 2006. Diffusion maps. Appl. Comput. Harmon. Anal. 21, 5–30. https://doi.org/10.1016/j.acha.2006.04.006.

Craddock, C., Sikka, S., Cheung, B., Khanuja, R., Ghosh, S.S., Yan, C., Li, Q., Lurie, D., Vogelstein, J., Burns, R., Colcombe, S., Mennes, M., Kelly, C., Martino, A.Di, Castellanos, F.X., Milham, M., 2013. Towards Automated Analysis of Connectomes: The Configurable Pipeline for the Analysis of Connectomes (C-PAC). Front. Neuroinform. https://doi.org/10.3389/conf.fninf.2013.09.00042.

Dale, A.M., Fischl, B., Sereno, M.I., 1999. Cortical surface-based analysis: I. Segmentation and surface reconstruction. Neuroimage 9, 179–194. https://doi.org/10.1006/nimg.1998.0395.

Damoiseaux, J.S., Greicius, M.D., 2009. Greater than the sum of its parts: A review of studies combining structural connectivity and resting-state functional connectivity. Brain Struct. Funct. 213, 525–533. https://doi.org/10.1007/s00429-009-0208-6.

Deco, G., Ponce-Alvarez, A., Mantini, D., Romani, G.L., Hagmann, P., Corbetta, M., 2013. Resting-state functional connectivity emerges from structurally and dynamically shaped slow linear fluctuations. J. Neurosci. 33, 11239–11252. https://doi.org/10.1523/JNEUROSCI.1091-13.2013.

Di Martino, A., O'Connor, D., Chen, B., Alaerts, K., Anderson, J.S., Assaf, M., Balsters, J. H., Baxter, L., Beggiato, A., Bernaerts, S., Blanken, L.M.E., Bookheimer, S.Y., Braden, B.B., Byrge, L., Castellanos, F.X., Dapretto, M., Delorme, R., Fair, D.A., Fishman, I., Fitzgerald, J., Gallagher, L., Keehn, R.J.J., Kennedy, D.P., Lainhart, J.E., Luna, B., Mostofsky, S.H., Müller, R.A., Nebel, M.B., Nigg, J.T., O'Hearn, K., Solomon, M., Toro, R., Vaidya, C.J., Wenderoth, N., White, T., Craddock, R.C., Lord, C., Leventhal, B., Milham, M.P., 2017. Enhancing studies of the connectome in autism using the autism brain imaging data exchange II. Sci. Data 4, 1–15. https://doi.org/10.1038/sdata.2017.10.

Di Martino, A., Yan, C.G., Li, Q., Denio, E., Castellanos, F.X., Alaerts, K., Anderson, J.S., Assaf, M., Bookheimer, S.Y., Dapretto, M., Deen, B., Delmonte, S., Dinstein, I., Ertl-Wagner, B., Fair, D.A., Gallagher, L., Kennedy, D.P., Keown, C.L., Keysers, C., Lainhart, J.E., Lord, C., Luna, B., Menon, V., Minshew, N.J., Monk, C.S., Mueller, S., Müller, R.A., Nebel, M.B., Nigg, J.T., O'Hearn, K., Pelphrey, K.A., Peltier, S.J., Rudie, J.D., Sunaert, S., Thioux, M., Tyszka, J.M., Uddin, L.Q., Verhoeven, J.S., Wenderoth, N., Wiggins, J.L., Mostofsky, S.H., Milham, M.P., 2014. The autism brain imaging data exchange: Towards a large-scale evaluation of the intrinsic brain architecture in autism. Mol. Psychiatry 19, 659–667. https://doi.org/10.1038/mp.2013.78.

Dickie, E.W., Ameis, S.H., Shahab, S., Calarco, N., Smith, D.E., Miranda, D., Viviano, J.D., Voineskos, A.N., 2018. Personalized Intrinsic Network Topography Mapping and Functional Connectivity Deficits in Autism Spectrum Disorder. Biol. Psychiatry 84, 278–286. https://doi.org/10.1016/j.biopsych.2018.02.1174.

Fan, F., Liao, X., Lei, T., Zhao, T., Xia, M., Men, W., Wang, Y., Hu, M., Liu, J., Qin, S., Tan, S., Gao, J.H., Dong, Q., Tao, S., He, Y., 2021. Development of the default-mode network during childhood and adolescence: A longitudinal resting-state fMRI study. Neuroimage 226, 117581. https://doi.org/10.1016/j.neuroimage.2020.117581.

Fischl, B., 2012. FreeSurfer. Neuroimage 62, 774–781. https://doi.org/10.1016/j.neuroimage.2012.01.021.

Fischl, B., Liu, A., Dale, A.M., 2001. Automated manifold surgery: Constructing geometrically accurate and topologically correct models of the human cerebral cortex. IEEE Trans. Med. Imaging 20, 70–80. https://doi.org/10.1109/42.906426.

Fischl, B., Sereno, M.I., Dale, A.M., 1999a. Cortical surface-based analysis: II. Inflation, flattening, and a surface-based coordinate system. Neuroimage 9, 195–207. https://doi.org/10.1006/nimg.1998.0396.

Fischl, B., Sereno, M.I., Tootell, R.B.H., Dale, A.M., 1999b. High-resolution inter-subject averaging and a surface-based coordinate system. Hum. Brain Mapp. 8, 272–284. https://doi.org/10.1002/(SICI)1097-0193(1999)8.

Fornito, A., Zalesky, A., Bullmore, E., 2016. Fundamentals of Brain Network Analysis. Academic Press, Amsterdam.

Geschwind, D.H., 2011. Genetics of autism spectrum disorders. Trends Cogn. Sci. 15, 409–416. https://doi.org/10.1016/j.tics.2011.07.003.

Goñi, J., Van Den Heuvel, M.P., Avena-Koenigsberger, A., De Mendizabal, N.V., Betzel, R. F., Griffa, A., Hagmann, P., Corominas-Murtra, B., Thiran, J.P., Sporns, O., 2014. Resting-brain functional connectivity predicted by analytic measures of network communication. Proc. Natl. Acad. Sci. U.S.A. 111, 833–838. https://doi.org/10.1073/pnas.1315529111.

Hahamy, A., Behrmann, M., Malach, R., 2015. The idiosyncratic brain: Distortion of spontaneous connectivity patterns in autism spectrum disorder. Nat. Neurosci. 18, 302–309. https://doi.org/10.1038/nn.3919.

Honey, C.J., Sporns, O., Cammoun, L., Gigandet, X., Thiran, J.P., Meuli, R., Hagmann, P., 2009. Predicting human resting-state functional connectivity from structural connectivity. Proc. Natl. Acad. Sci. U.S.A. 106, 2035–2040. https://doi.org/10.1073/pnas.0811168106.

Hong, S.J., Hyung, B., Paquola, C., Bernhardt, B.C., 2019b. The Superficial White Matter in Autism and Its Role in Connectivity Anomalies and Symptom Severity. Cereb. Cortex 29, 4415–4425. https://doi.org/10.1093/cercor/bhy321.

Hong, S.J., Mottron, L., Park, B., Benkarim, O., Valk, S.L., Paquola, C., Larivière, S., Vos de Wael, R., Degré-Pelletier, J., Soulieres, I., Ramphal, B., Margolis, A., Milham, M., Di Martino, A., Bernhardt, B.C., 2022. A convergent structure–function substrate of cognitive imbalances in autism. Cereb. Cortex 1–15. https://doi.org/10.1093/cercor/bhac156.

Hong, S.J., Valk, S.L., Di Martino, A., Milham, M.P., Bernhardt, B.C., 2018. Multidimensional neuroanatomical subtyping of autism spectrum disorder. Cereb. Cortex 28, 3578–3588. https://doi.org/10.1093/cercor/bhx229.

Hong, S.J., Vogelstein, J.T., Gozzi, A., Bernhardt, B.C., Yeo, B.T.T., Milham, M.P., Di Martino, A., 2020. Toward Neurosubtypes in Autism. Biol. Psychiatry 88, 111–128. https://doi.org/10.1016/j.biopsych.2020.03.022.

Hong, S.J., Vos De Wael, R., Bethlehem, R.A.I., Lariviere, S., Paquola, C., Valk, S.L., Milham, M.P., Martino, A.Di, Margulies, D.S., Smallwood, J., Bernhardt, B.C., 2019a. Atypical functional connectome hierarchy in autism. Nat. Commun. 10, 1022.

Hull, J.V., Jacokes, Z.J., Torgerson, C.M., Irimia, A., Van Horn, J.D., Aylward, E., Bernier, R., Bookheimer, S., Dapretto, M., Gaab, N., Geschwind, D., Jack, A., Nelson, C., Pelphrey, K., State, M., Ventola, P., Webb, S.J., 2017. Resting-state functional connectivity in autism spectrum disorders: A review. Front. Psychiatry 7. https://doi.org/10.3389/fpsyt.2016.00205.

Huntenburg, J.M., Bazin, P.L., Margulies, D.S., 2018. Large-Scale Gradients in Human Cortical Organization. Trends Cogn. Sci. https://doi.org/10.1016/j.tics.2017.11.002.

Hutsler, J.J., Love, T., Zhang, H., 2007. Histological and Magnetic Resonance Imaging Assessment of Cortical Layering and Thickness in Autism Spectrum Disorders. Biol. Psychiatry 61, 449–457. https://doi.org/10.1016/j.biopsych.2006.01.015.

Hutsler, J.J., Zhang, H., 2010. Increased dendritic spine densities on cortical projection neurons in autism spectrum disorders. Brain Res. 1309, 83–94. https://doi.org/10.1016/j.brainres.2009.09.120.

Jeurissen, B., Tournier, J.D., Dhollander, T., Connelly, A., Sijbers, J., 2014. Multi-tissue constrained spherical deconvolution for improved analysis of multi-shell diffusion MRI data. Neuroimage 103, 411–426. https://doi.org/10.1016/j.neuroimage.2014.07.061.

Kana, R.K., Uddin, L.Q., Kenet, T., Chugani, D., Müller, R.A., 2014. Brain connectivity in autism. Front. Hum. Neurosci. 8, 8–11. https://doi.org/10.3389/fnhum.2014.00349.

Kharabian Masouleh, S., Plachti, A., Hoffstaedter, F., Eickhoff, S., Genon, S., 2020. Characterizing the gradients of structural covariance in the human hippocampus. Neuroimage 218, 116972. https://doi.org/10.1016/j.neuroimage.2020.116972.
Krishnan, A., Williams, L.J., McIntosh, A.R., Abdi, H., 2011. Partial Least Squares (PLS) methods for neuroimaging: a tutorial and review. Neuroimage 56, 455–475. https://doi.org/10.1016/j.neuroimage.2010.07.034.
Larivière, S., Bayrak, Ş., Vos de Wael, R., Benkarim, O., Herholz, P., Rodriguez-Cruces, R., Paquola, C., Hong, S.J., Misic, B., Evans, A.C., Valk, S.L., Bernhardt, B.C., 2023. BrainStat: A toolbox for brain-wide statistics and multimodal feature associations. Neuroimage 266. https://doi.org/10.1016/j.neuroimage.2022.119807.
Larivière, S., Paquola, C., Park, B., Royer, J., Wang, Y., Benkarim, O., Vos de Wael, R., Valk, S.L., Thomopoulos, S.I., Kirschner, M., Lewis, L.B., Evans, A.C., Sisodiya, S.M., McDonald, C.R., Thompson, P.M., Bernhardt, B.C., 2021. The ENIGMA Toolbox: multiscale neural contextualization of multisite neuroimaging datasets. Nat. Methods. https://doi.org/10.1038/s41592-021-01186-4.
Leech, R., Vos De Wael, R., Váša, F., Xu, T., Austin Benn, R., Scholz, R., Braga, R.M., Milham, M.P., Royer, J., Bernhardt, B.C., Jones, E.J.H., Jefferies, E., Margulies, D.S., Smallwood, J., 2023. Variation in spatial dependencies across the cortical mantle discriminates the functional behaviour of primary and association cortex. Nat. Commun. 14 https://doi.org/10.1038/s41467-023-41334-2.
Lord, C., Risi, S., Lambrecht, L., Cook, E.H., Leventhal, B.L., Dilavore, P.C., Pickles, A., Rutter, M., 2000. The Autism Diagnostic Observation Schedule-Generic: A standard measure of social and communication deficits associated with the spectrum of autism. J. Autism Dev. Disord. 30, 205–223. https://doi.org/10.1023/A:1005592401947.
Lord, C., Rutter, M., Couteur, A.Le, 1994. Autism Diagnostic Interview-Revised: A revised version of a diagnostic interview for caregivers of individuals with possible pervasive developmental disorders. J. Autism Dev. Disord. 24, 659–685. https://doi.org/10.1007/BF02172145.
Margulies, D.S., Ghosh, S.S., Goulas, A., Falkiewicz, M., Huntenburg, J.M., Langs, G., Bezgin, G., Eickhoff, S.B., Castellanos, F.X., Petrides, M., Jefferies, E., Smallwood, J., 2016. Situating the default-mode network along a principal gradient of macroscale cortical organization. Proc. Natl. Acad. Sci. U.S.A. 113, 12574–12579. https://doi.org/10.1073/pnas.1608282113.
Markello, R.D., Misic, B., 2021. Comparing spatial null models for brain maps. Neuroimage 236, 118052. https://doi.org/10.1016/j.neuroimage.2021.118052.
Mars, R.B., Neubert, F.X., Noonan, M.A.P., Sallet, J., Toni, I., Rushworth, M.F.S., 2012. On the relationship between the "default mode network" and the "social brain. Front. Hum. Neurosci. 6, 1–9. https://doi.org/10.3389/fnhum.2012.00189.
Martínez-Cerdeño, V., 2017. Dendrite and spine modifications in autism and related neurodevelopmental disorders in patients and animal models. Dev. Neurobiol. 77, 393–404. https://doi.org/10.1002/dneu.22417.
McIntosh, A.R., Mišić, B., 2013. Multivariate statistical analyses for neuroimaging data. Annu. Rev. Psychol. 64, 499–525. https://doi.org/10.1146/annurev-psych-113011-143804.
McKavanagh, R., Buckley, E., Chance, S.A., 2015. Wider minicolumns in autism: A neural basis for altered processing? Brain 138, 2034–2045. https://doi.org/10.1093/brain/awv110.
Mckeown, B., Strawson, W.H., Wang, H.T., Karapanagiotidis, T., Vos de Wael, R., Benkarim, O., Turnbull, A., Margulies, D., Jefferies, E., McCall, C., Bernhardt, B., Smallwood, J., 2020. The relationship between individual variation in macroscale functional gradients and distinct aspects of ongoing thought. Neuroimage 220, 117072. https://doi.org/10.1016/j.neuroimage.2020.117072.
Mesulam, M.M., 1998. From sensation to cognition. Brain 121, 1013–1052. https://doi.org/10.1093/brain/121.6.1013.
Mišic, B., Betzel, R.F., De Reus, M.A., Van Den Heuvel, M.P., Berman, M.G., McIntosh, A.R., Sporns, O., 2016. Network-level structure-function relationships in human neocortex. Cereb. Cortex 26, 3285–3296. https://doi.org/10.1093/cercor/bhw089.
Mottron, L., Dawson, M., Soulières, I., Hubert, B., Burack, J., 2006. Enhanced perceptual functioning in autism: An update, and eight principles of autistic perception. J. Autism Dev. Disord. 36, 27–43. https://doi.org/10.1007/s10803-005-0040-7.
Müller, R.A., Shih, P., Keehn, B., Deyoe, J.R., Leyden, K.M., Shukla, D.K., 2011. Underconnected, but how? A survey of functional connectivity MRI studies in autism spectrum disorders. Cereb. Cortex 21, 2233–2243. https://doi.org/10.1093/cercor/bhq296.
Murphy, C., Wang, H.T., Konu, D., Lowndes, R., Margulies, D.S., Jefferies, E., Smallwood, J., 2019. Modes of operation: A topographic neural gradient supporting stimulus dependent and independent cognition. Neuroimage 186, 487–496. https://doi.org/10.1016/j.neuroimage.2018.11.009.
Padmanabhan, A., Lynch, C.J., Schaer, M., Menon, V., 2017. The Default Mode Network in Autism. Biol. Psychiatry Cogn. Neurosci. Neuroimaging 2, 476–486. https://doi.org/10.1016/j.bpsc.2017.04.004.
Paquola, C., Amunts, K., Evans, A., Smallwood, J., Bernhardt, B., 2022. Closing the mechanistic gap: the value of microarchitecture in understanding cognitive networks. Trends Cogn. Sci. 26, 873–886. https://doi.org/10.1016/j.tics.2022.07.001.
Paquola, C., Seidlitz, J., Benkarim, O., Royer, J., Klimes, P., Bethlehem, R.A.I., Larivière, S., Vos de Wael, R., Rodríguez-Cruces, R., Hall, J.A., Frauscher, B., Smallwood, J., Bernhardt, B.C., 2020. A multi-scale cortical wiring space links cellular architecture and functional dynamics in the human brain. PLoS Biol. https://doi.org/10.1371/journal.pbio.3000979.
Paquola, C., Vos De Wael, R., Wagstyl, K., Bethlehem, R.A.I., Hong, S.J., Seidlitz, J., Bullmore, E.T., Evans, A.C., Misic, B., Margulies, D.S., Smallwood, J., Bernhardt, B.C., 2019. Microstructural and functional gradients are increasingly dissociated in transmodal cortices. PLoS Biol. 17, e3000284 https://doi.org/10.1371/journal.pbio.3000284.
Park, B., Bethlehem, R.A.I., Paquola, C., Larivière, S., Rodríguez-Cruces, R., Vos de Wael, R., Bullmore, E., Dolan, R., Goodyer, I., Fonagy, P., Jones, P., Moutoussis, M., Hauser, T., Neufeld, S., Romero-Garcia, R., St Clair, M., Vértes, P., Whitaker, K., Inkster, B., Prabhu, G., Ooi, C., Toseeb, U., Widmer, B., Bhatti, J., Villis, L., Alrumaithi, A., Birt, S., Bowler, A., Cleridou, K., Dadabhoy, H., Davies, E., Firkins, A., Granville, S., Harding, E., Hopkins, A., Isaacs, D., King, J., Kokorikou, D., Maurice, C., McIntosh, C., Memarzia, J., Mills, H., O'Donnell, C., Pantaleone, S., Scott, J., Kiddle, B., Polek, E., Fearon, P., Suckling, J., van Harmelen, A.L., Kievit, R., Chamberlain, S., Bullmore, E.T., Bernhardt, B.C., 2021a. An expanding manifold in transmodal regions characterizes adolescent reconfiguration of structural connectome organization. eLife 10, e64694. https://doi.org/10.7554/eLife.64694.
Park, B., Hong, S., Valk, S.L., Paquola, C., Benkarim, O., Bethlehem, R.A.I., Di Martino, A., Milham, M.P., Gozzi, A., Yeo, B.T.T., Smallwood, J., Bernhardt, B.C., 2021b. Differences in subcortico-cortical interactions identified from connectome and microcircuit models in autism. Nat. Commun. https://doi.org/10.1038/s41467-021-21732-0.
Park, B., Paquola, C., Bethlehem, R.A.I., Benkarim, O., Mišić, B., Smallwood, J., Bullmore, E.T., Bernhardt, B.C., Bullmore, E., Dolan, R., Goodyer, I., Fonagy, P., Jones, P., Moutoussis, M., Hauser, T., Neufeld, S., Romero-Garcia, R., St Clair, M., Vértes, P., Whitaker, K., Inkster, B., Prabhu, G., Ooi, C., Toseeb, U., Widmer, B., Bhatti, J., Villis, L., Alrumaithi, A., Birt, S., Bowler, A., Cleridou, K., Dadabhoy, H., Davies, E., Firkins, A., Granville, S., Harding, E., Hopkins, A., Isaacs, D., King, J., Kokorikou, D., Maurice, C., McIntosh, C., Memarzia, J., Mills, H., O'Donnell, C., Pantaleone, S., Scott, J., Kiddle, B., Polek, E., Fearon, P., Suckling, J., van Harmelen, A.L., Kievit, R., Chamberlain, S., 2022. Adolescent development of multiscale structural wiring and functional interactions in the human connectome. Proc. Natl. Acad. Sci. U. S. A. 119, e2116673119 https://doi.org/10.1073/pnas.2116673119.
Park, B., Park, H., Morys, F., Kim, M., Byeon, K., Lee, H., Kim, S.H., Valk, S.L., Dagher, A., Bernhardt, B.C., 2021c. Inter-individual body mass variations relate to fractionated functional brain hierarchies. Commun. Biol. 4, 1–12. https://doi.org/10.1038/s42003-021-02268-x.
Park, B., Vos de Wael, R., Paquola, C., Larivière, S., Benkarim, O., Royer, J., Tavakol, S., Cruces, R.R., Li, Q., Valk, S.L., Margulies, D.S., Mišić, B., Bzdok, D., Smallwood, J., Bernhardt, B.C., 2021d. Signal diffusion along connectome gradients and inter-hub routing differentially contribute to dynamic human brain function. Neuroimage 224, 117429. https://doi.org/10.1016/j.neuroimage.2020.117429.
Power, J.D., Barnes, K.A., Snyder, A.Z., Schlaggar, B.L., Petersen, S.E., 2012. Spurious but systematic correlations in functional connectivity MRI networks arise from subject motion. Neuroimage 59, 2142–2154. https://doi.org/10.1016/j.neuroimage.2011.10.018.
Power, J.D., Mitra, A., Laumann, T.O., Snyder, A.Z., Schlaggar, B.L., Petersen, S.E., 2014. Methods to detect, characterize, and remove motion artifact in resting state fMRI. Neuroimage 84, 320–341. https://doi.org/10.1016/j.neuroimage.2013.08.048.
Quesnel-Vallières, M., Weatheritt, R.J., Cordes, S.P., Blencowe, B.J., 2019. Autism spectrum disorder: insights into convergent mechanisms from transcriptomics. Nat. Rev. Genet. 20, 51–63. https://doi.org/10.1038/s41576-018-0066-2.
Raichle, M.E., 2015. The Brain's Default Mode Network. Annu. Rev. Neurosci. 38, 433–447. https://doi.org/10.1146/annurev-neuro-071013-014030.
Rosenthal, G., Váša, F., Griffa, A., Hagmann, P., Amico, E., Goñi, J., Avidan, G., Sporns, O., 2018. Mapping higher-order relations between brain structure and function with embedded vector representations of connectomes. Nat. Commun. 9, 2178. https://doi.org/10.1038/s41467-018-04614-w.
Rylaarsdam, L., Guemez-Gamboa, A., 2019. Genetic Causes and Modifiers of. Front. Cell Neurosci. 13, 385. https://doi.org/10.3389/fncel.2019.00385.
Schaefer, A., Kong, R., Gordon, E.M., Laumann, T.O., Zuo, X.N., Holmes, A.J., Eickhoff, S. B., Yeo, B.T.T., 2018. Local-Global Parcellation of the Human Cerebral Cortex from Intrinsic Functional Connectivity MRI. Cereb. Cortex 28, 3095–3114. https://doi.org/10.1093/cercor/bhx179.
Ségonne, F., Pacheco, J., Fischl, B., 2007. Geometrically accurate topology-correction of cortical surfaces using nonseparating loops. IEEE Trans. Med. Imaging 26, 518–529. https://doi.org/10.1109/TMI.2006.887364.
Seguin, C., Razi, A., Zalesky, A., 2019. Inferring neural signalling directionality from undirected structural connectomes. Nat. Commun. 10, 4289. https://doi.org/10.1038/s41467-019-12201-w.
Seguin, C., Van Den Heuvel, M.P., Zalesky, A., 2018. Navigation of brain networks. Proc. Natl. Acad. Sci. U.S.A. 115, 6297–6302. https://doi.org/10.1073/pnas.1801351115.
Simms, M.L., Kemper, T.L., Timbie, C.M., Bauman, M.L., Blatt, G.J., 2009. The anterior cingulate cortex in autism: Heterogeneity of qualitative and quantitative cytoarchitectonic features suggests possible subgroups. Acta Neuropathol. 118, 673–684. https://doi.org/10.1007/s00401-009-0568-2.
Smallwood, J., Bernhardt, B.C., Leech, R., Bzdok, D., Jefferies, E., Margulies, D.S., 2021. The default mode network in cognition: a topographical perspective. Nat. Rev. Neurosci. 22, 503–513. https://doi.org/10.1038/s41583-021-00474-4.
Smith, R.E., Tournier, J.D., Calamante, F., Connelly, A., 2015. SIFT2: Enabling dense quantitative assessment of brain white matter connectivity using streamlines tractography. Neuroimage 119, 338–351. https://doi.org/10.1016/j.neuroimage.2015.06.092.
Smith, R.E., Tournier, J.D., Calamante, F., Connelly, A., 2012. Anatomically-constrained tractography: Improved diffusion MRI streamlines tractography through effective use of anatomical information. Neuroimage 62, 1924–1938. https://doi.org/10.1016/j.neuroimage.2012.06.005.
Snyder, A.Z., Bauer, A.Q., 2019. Mapping Structure-Function Relationships in the Brain. Biol. Psychiatry Cogn. Neurosci. Neuroimaging 4, 510–521. https://doi.org/10.1016/j.bpsc.2018.10.005.

Suárez, L.E., Markello, R.D., Betzel, R.F., Misic, B., 2020. Linking Structure and Function in Macroscale Brain Networks. Trends Cogn. Sci. 24, 302–315. https://doi.org/10.1016/j.tics.2020.01.008.

Sydnor, V.J., Larsen, B., Bassett, D.S., Alexander-Bloch, A., Fair, D.A., Liston, C., Mackey, A.P., Milham, M.P., Pines, A., Roalf, D.R., Seidlitz, J., Xu, T., Raznahan, A., Satterthwaite, T.D., 2021. Neurodevelopment of the association cortices: Patterns, mechanisms, and implications for psychopathology. Neuron 109, 2820–2846. https://doi.org/10.1016/j.neuron.2021.06.016.

Takahashi, T., Yoshimura, Y., Hiraishi, H., Hasegawa, C., Munesue, T., Higashida, H., Minabe, Y., Kikuchi, M., 2016. Enhanced brain signal variability in children with autism spectrum disorder during early childhood. Hum. Brain Mapp. 37, 1038–1050. https://doi.org/10.1002/hbm.23089.

Tenenbaum, J.B., Silva, V.de, Langford, J.C., 2000. A Global Geometric Framework for Nonlinear Dimensionality Reduction. Science 290, 2319–2323. https://doi.org/10.1126/science.290.5500.2319 (80-.).

Thompson, W.H., Fransson, P., 2016. On Stabilizing the Variance of Dynamic Functional Brain Connectivity Time Series. Brain Connect. 6, 735–746. https://doi.org/10.1089/brain.2016.0454.

Tian, Y., Margulies, D.S., Breakspear, M., Zalesky, A., 2020. Topographic organization of the human subcortex unveiled with functional connectivity gradients. Nat. Neurosci. 23, 1421–1432. https://doi.org/10.1038/s41593-020-00711-6.

Tournier, J.D., Calamante, F., Connelly, A., 2010. Improved probabilistic streamlines tractography by 2 nd order integration over fibre orientation distributions. In: Proceedings of the International Society for Magnetic Resonance in Medicine, p. 1670.

Tournier, J.D., Calamante, F., Connelly, A., 2012. MRtrix: Diffusion tractography in crossing fiber regions. Int. J. Imaging Syst. Technol. 22, 53–66. https://doi.org/10.1002/ima.22005.

Tournier, J.D., Smith, R., Raffelt, D., Tabbara, R., Dhollander, T., Pietsch, M., Christiaens, D., Jeurissen, B., Yeh, C.H., Connelly, A., 2019. MRtrix3: A fast, flexible and open software framework for medical image processing and visualisation. Neuroimage 202, 116137. https://doi.org/10.1016/j.neuroimage.2019.116137.

Townsend, J., Koep, N., Weichwald, S., 2016. Pymanopt: A python toolbox for optimization on manifolds using automatic differentiation. J. Mach. Learn Res. 17, 1–5.

Uddin, L.Q., Supekar, K., Lynch, C.J., Cheng, K.M., Odriozola, P., Barth, M.E., Phillips, J., Feinstein, C., Abrams, D.A., Menon, V., 2015. Brain state differentiation and behavioral inflexibility in autism. Cereb. Cortex 25, 4740–4747. https://doi.org/10.1093/cercor/bhu161.

Uddin, L.Q., Supekar, K., Menon, V., 2013. Reconceptualizing functional brain connectivity in autism from a developmental perspective. Front. Hum. Neurosci. 7, 1–11. https://doi.org/10.3389/fnhum.2013.00458.

Valk, S.L., Xu, T., Paquola, C., Park, B., Bethlehem, R.A.I., Vos de Wael, R., Royer, J., Masouleh, S.K., Bayrak, Ş., Kochunov, P., Yeo, B.T.T., Margulies, D., Smallwood, J., Eickhoff, S.B., Bernhardt, B.C., 2022. Genetic and phylogenetic uncoupling of structure and function in human transmodal cortex. Nat. Commun. 13, 2341. https://doi.org/10.1038/s41467-022-29886-1.

Van Essen, D.C., Smith, S.M., Barch, D.M., Behrens, T.E.J., Yacoub, E., Ugurbil, K., 2013. The WU-Minn Human Connectome Project: an overview. Neuroimage 80, 62–79. https://doi.org/10.1016/j.neuroimage.2013.05.041.

Vázquez-Rodríguez, B., Suárez, L.E., Markello, R.D., Shafiei, G., Paquola, C., Hagmann, P., Van Den Heuvel, M.P., Bernhardt, B.C., Spreng, R.N., Misic, B., 2019. Gradients of structure–function tethering across neocortex. Proc. Natl. Acad. Sci. U. S.A. 116, 21219–21227. https://doi.org/10.1073/pnas.1903403116.

von Luxburg, U., 2007. A tutorial on spectral clustering. Stat. Comput. 17, 395–416. https://doi.org/10.1007/s11222-007-9033-z.

Vos de Wael, R., Benkarim, O., Paquola, C., Lariviere, S., Royer, J., Tavakol, S., Xu, T., Hong, S.J., Valk, S.L., Misic, B., Milham, M.P., Margulies, D.S., Smallwood, J., Bernhardt, B.C., 2020. BrainSpace: a toolbox for the analysis of macroscale gradients in neuroimaging and connectomics datasets. Commun. Biol. 3, 103. https://doi.org/10.1038/s42003-020-0794-7.

Wang, P., Kong, R., Kong, X., Liégeois, R., Orban, C., Deco, G., Van Den Heuvel, M.P., Yeo, B.T.T., 2019. Inversion of a large-scale circuit model reveals a cortical hierarchy in the dynamic resting human brain. Sci. Adv. 5, eaat7854. https://doi.org/10.1126/sciadv.aat7854.

Worsley, K.J., Taylor, J.E., Carbonell, Chung, M.K., Duerden, E., Bernhardt, B., Lyttelton, O., Boucher, M., Evans, A.C., 2009. SurfStat: A Matlab toolbox for the statistical analysis of univariate and multivariate surface and volumetric data using linear mixed effects models and random field theory. Neuroimage 47, S102. https://doi.org/10.1016/S1053-8119(09)70882-1.

Yeo, B.T.T., Krienen, F.M., Sepulcre, J., Sabuncu, M.R., Lashkari, D., Hollinshead, M., Roffman, J.L., Smoller, J.W., Zollei, L., Polimeni, J.R., Fischl, B., Liu, H., Buckner, R. L., 2011. The organization of the human cerebral cortex estimated by intrinsic functional connectivity. J. Neurophysiol. 106, 1125–1165. https://doi.org/10.1152/jn.00338.2011.

Zeighami, Y., Fereshtehnejad, S.M., Dadar, M., Collins, D.L., Postuma, R.B., Mišić, B., Dagher, A., 2019. A clinical-anatomical signature of Parkinson's disease identified with partial least squares and magnetic resonance imaging. Neuroimage 190, 69–78. https://doi.org/10.1016/j.neuroimage.2017.12.050.